Energy and exergy analysis of parallel flow double effect H$_2$O-[mmim][DMP] absorption refrigeration system for solar powered district cooling

M. Salim Ferwati [a,*], Ahmad Mohammad Ahmad [a],
Gorakshnath Dadabhau Takalkar [a,c,**], Yusuf Bicer [b]

[a] *College of Engineering, Qatar University, PO Box 2713, Doha, Qatar*
[b] *Division of Sustainable Development (DSD), College of Science and Engineering (CSE), Hamad Bin Khalifa University (HBKU), Qatar Foundation (QF), Education City, Doha, Qatar*
[c] *Fiber Research Center, (A Unit of Grasim Industries Limited - Aditya Birla Group) Kharach, Kosamba, Dist Bharuch, Gujarat, India*

A B S T R A C T

Solar thermal energy-driven double effect absorption refrigeration system (DE-ARS) for district cooling in smart cities is an efficient, and sustainable alternative for centralized air conditioning and concurrently harnesses low-grade solar energy. This work investigates ionic liquid based H$_2$O-[mmim][DMP] mixture as an alternative working fluid to overcome the drawback of H$_2$O–LiBr driven DE-ARS. The thermodynamic properties of H$_2$O-[mmim][DMP] mixture is evaluated using the excess Gibbs free energy model. Performance modeling and simulation of DE-ARS is based on both energy and exergy analysis by applying the first and second laws of thermodynamic. The performance, and solution circulation ratio of parallel flow DE-ARS is assessed and optimized under various temperatures and solution distribution ratios. In comparison to the conventional H$_2$O–LiBr, the proposed H$_2$O-[mmim][DMP] working fluid achieves 5.22% and 4.95% improvement in COP and ECOP, respectively at T$_h$/T$_e$/T$_a$/T$_c$ of 140/5/30/30°C . An optimization of generator temperature to achieve maximum COP and ECOP is performed for a wide range of evaporation temperature from 5 to 20°C and T$_a$/T$_c$ from 30 to 40°C. An optimization of H$_2$O-[mmim][DMP] mixture driven DE-ARS reveals the uppermost COP$_{max}$ and ECOP$_{max}$ of 1.81 and 0.69 for T$_e$ of 20°C and T$_a$=T$_c$=30°C.

1. Introduction

Emission of greenhouse gases (CO$_2$, CH$_4$, etc.) into the atmosphere is causing a global warming effect on the earth's atmosphere due to the rise in primary consumption obtained from non-renewable fossil fuels. Future relevance in energy saving, CO$_2$ mitigation, and reduction in greenhouse gases by exploiting renewable energy resources is essential to adopt for sustainability and climate change [1]. Worldwide large number of people lives in cities wherein electricity demand for space cooling and heating is enormous, and the future electricity demand of emerging smart cities due to rapid development may grow up. Therefore, the energy security for upcoming cities

must be sustainable and efficient to fulfil daily energy-dependent building utilities like lighting, cooling, and heating [2]. Overall, more than 50% of building energy is utilized to fulfil the cooling and heating demand. Especially in the Middle Eastern GCC countries, the cooling demand of the building sector is more due to high ambient temperature [3–6]. In such a case, centralized district cooling (DC) processes via absorption refrigeration system (ARS) is one of the potential alternate to harness renewable solar energy for air-conditioning of building [7–10]. Wide literature studies on the solar cooling have been reported and suggest that solar energy has enormous potential on heating, cooling and refrigeration on large scale [7,11,12]. The centralized chiller plant and associated chilled water distribution network (called as district cooling) have been employed to fulfil the space cooling demand of populated cities [13]. Zheng et al. [14] have investigated solar parabolic trough collector integrated ARS for space cooling and heating and confirmed the benefits with a reduction in CO_2 emission by 18.8%. Consequently, the solar-driven space cooling process has a favorable prospect in sustainable development due to independence on fossil fuel, commercial feasibility, and environment friendliness to reduce CO_2 emission.

Compared to standalone electric driven vapor compression cooling units, the centralized DC process reduces water usage and electricity consumption by up to 65%. Additionally, the high-grade energy consumption is reduced through the heat-driven absorption refrigeration technology by utilization of low-temperature heat obtained via waste heat and renewable sources like solar, geothermal, biomass, etc. [15,16]. Ultimately, thermal-driven ARS reduces the consumption of high-grade electricity, incurred operating cost and support the sustainability, including mitigation of CO_2 emission [17,18].

In this, overall efficiency of heat-driven absorption cooling and refrigeration system varies with the type of working mixture utilized, absorption cycle configuration (single, double, triple effect cycle), and operating conditions within the evaporator, generator, absorber, and condenser [5,9,19,20]. Commercially two working fluids; NH_3–H_2O and H_2O–LiBr have been accepted widely for cooling and refrigeration [21,22]; the major impediment of these working pairs are toxicity, high pressure, and rectification for NH_3–H_2O and crystallization and corrosion for H_2O–LiBr. Such shortcoming urges researchers to rediscover novel alternative potential working fluids for efficient utilization and conversion of low-grade heat below $200°C$[23] as proposed in this work.

Recently, numerous ionic liquids (IL) have been proposed as an adsorbent in combination with a refrigerant like water, hydro-carbon, ammonia [24]. These ILs have been examined by researchers intensively; to find a better option for replacing H_2O–LiBr mixture by overcoming the corrosion and crystallization issue [25–34]. ILs' main beneficial properties are enhanced solubility, better thermal stability, adaptable thermodynamics properties due to the combination of cation and anion, low vapor pressure, liquid state that eludes the crystallization and less corrosive [27,28,35–39]. In specific, the mixture of IL with green and natural refrigerant water as a working fluid has been widely investigated as an alternative to LiBr–H_2O for air conditioning and cooling purposes [33].

Sun et al. [27] have analyzed refrigerant R1234yf, and six ILs for single effect and compression assisted ARS. The cyclic thermal performance of [hmim][Tf2N] was found to be better with six IL-based absorbents but lower than conventional working fluids due to the low specific volume of R1234yf. Likewise, Kim and Kohl [40] modeled and simulated the performance of [hmim][PF6] and [hmim][Tf2N] with R134a refrigerant combination for ARS wherein [hmim][Tf2N] showed better COP in most input operating conditions. Refrigerant CO_2 with [emim][Tf2N] based compression-assisted ARS was investigated by Li et al. [26] and they found that CO_2 pressure and temperature were essential for enhancement and optimizing ARS outcomes. Likewise, Wang et al. [37] have assessed the performance of IL-based ternary mixture $LiNO_3$-[BMIM]NO_3/H_2O for hybrid compression ARS with the measurement of ther-modynamics properties and corrosion. Their results showed a better performance for the proposed ternary mixture driven hybrid ARS with utilization low generator temperature in alternative to conventional LiBr–H_2O.

Wu et al. [41] have investigated different ILs for thermal energy storage purposes and simulation showed that [DMIM][DMP] generated better thermal COP of 0.745. However ionic liquid [EMIM] [Ac] expressed maximum thermal energy storage density of 87.5 kW/m^3. Further Wu et al. [42] explored low and high pressure compressor assisted hybrid single effect absorption system using various combination of refrigerant and ILs (R134a/[HMIM][Tf2N], R32/[HMIM][Tf2N],R152a/[HMIM][Tf2N], R161/[HMIM][Tf2N], R1234yf/[HMIM][Tf2N], R1234ze/[HMIM][Tf2N]). Overall, in those working fluids, the COP of R32/[HMIM][Tf2N] was found to be better in single effect low-pressure compressor assisted ARS. Wang et al. [28] evaluated the selection criteria of vapor-liquid equi-librium models using IL-refrigerant binary mixture namely H_2O/[emim][DMP] and NH_3/[bmim][BF$_4$] combination for ARS and recommended the Redlich-Kwong EOS model for correlating VLE data and estimating mixing enthalpies of a binary mixture.

Two ARS configurations, namely single effect (SE) and double effect (DE) have been widely studied in the literature due to the utilization of heat below $200°C$ wherein DE-ARS gives higher COP [43]. Avanessian and Ameri [44] have performed a detailed economic survey of single and double effect ARS wherein; they concluded the DE-ARS is more economical with a low payback period and more sustainable with low CO_2 emission. SE-ARS is efficient to use low-grade heat source temperature below $100°C$. However, DE-ARS becomes more efficient (80% higher than SE-ARS) with the utilization of low-grade heat below $200°C$[45]. To predict the performance based on energy and exergy analysis, LiBr–H_2O based DE-ARS have been researched extensively for parallel and series solution flow configurations. In these DE-ARS, parallel flow of feed solution from absorber to the generators demonstrated better COP than series flow [46,47].

Farshi and Asadi [48] compared the energetic and exergetic COP of DE-ARS using two working pairs NH_3/$LiNO_3$ and NH_3/NaSCN towards utilization of low heat source and their thermodynamic simulation demonstrated high efficiency for wide range of crystal-lization of NH_3/$LiNO_3$ in compared to the NH_3/NaSCN. Dong et al. [49] and Takalkar et al. [50] have investigated thermodynamic properties of H_2O/1,3-dimethyl imidazolium dimethyl phosphate ([mmim] [DMP]) system. Their simulation results of single effect ARS using conventional LiBr–H_2O and proposed H_2O-[mmim][DMP] demonstrated better performance for H_2O-[mmim][DMP] mixture. However, their work is limited to single effect ARS. In comparison to LiBr–H_2O, H_2O-[mmim][DMP] enlarges the corrosion and crystallization range and it generates more attention for double effect ARS.

The literature completely lacks the performance analysis of the double effect ARS using promising IL based H_2O-[mmim][DMP]

mixture as an alternative working fluid. Therefore, the present work deals with the performance evaluation and heat source optimization of parallel flow DE-ARS using H_2O-[mmim][DMP] mixture as a working pair. Accordingly, this study investigates energetic and exergetic performances of DE-ARS components for wide temperatures wherein exergy analysis is based on the second law of thermodynamics and essential tool to identify the potential improvements in ARS [51–53] by considering the quality of energy. The effects of operating temperatures of evaporator (T_e), generator (T_g), absorber (T_a) and condenser (T_c) with solution distribution ratio (SDR) on the energetic (COP) and exergetic (ECOP) coefficient performances of DE-ARS were assessed in detail and also compared with the commercial working fluid H_2O–LiBr. Optimization of generator temperature (T_h) to achieve maximum COP and maximum ECOP was also investigated for different evaporation temperatures ($T_e = 5, 10, 15, 20\,^\circ C$), and three sink temperatures ($T_a = T_c = 30, 35, 40\,^\circ C$).

2. Parallel flow double effect absorption refrigeration system

Fig. 1 illustrates the H_2O-[mmim][DMP] mixture based double effect (or two-stage) parallel flow ARS used for performance simulation. The cooling cycle consists mainly of two generators (namely high (HTG) and low (LTG) temperature generator), two solution heat exchangers (SHE-LT, SHE-HT), evaporator, absorber, condenser, expansion valves, and solution pump. In this, refrigerant water vapor is generated in two stages at two different generator temperature and pressure in HTG and LTG of DE-ARS. In the cyclic operation, a weak solution of H_2O-[mmim][DMP] mixture (3) from the absorber is pumped and distributed into two parallel feed streams (11,12) to HTG and LTG, respectively. Solution heat recovery exchangers namely, SHE-LT and SHE-HT, recuperate the heat in between hot (strong solution) and cold (weak solution) streams. External heat obtained from the solar collector is provided to HTG, wherein high-pressure and high-temperature refrigerant water vapor (17) departs from the weak solution (stream 13). Then, water vapor is condensed within low-pressure LTG and the latent heat of condensation of refrigerant water within LTG is utilized as source of heat and to generate more extra refrigerant water vapor (7) from the second parallel feed weak solution (11). Refrigerant water vapor produced within LTG (7) is condensed within condenser, and latent heat of condensation is dissipated to ambient air either water-cooled or air-cooled type condenser. Further, high-pressure refrigerant water (8) is expanded through an expansion valve into low pressure (9) and then used as feed to the evaporator wherein cooling effect is delivered. The cooling with the evaporation of refrigerant water is achieved with the gain of heat from the space (or building) to be cooled (10). Strong H_2O-[mmim][DMP] solution from the bottom of HTG (14,15,16) and LTG (6) after heat recovery within SHE (SHE-LT, SHE-HT) is mixed (6) into low-pressure water vapor (10) and passed as top feed to the absorber. In the end, weak H_2O-[mmim][DMP] solution (1) is generated at the bottom of the absorber after the absorption of water vapor into strong H_2O-[mmim][DMP] solution. Heat of the absorption was removed through the dissipation of heat to ambient air. Formed weak H_2O-[mmim][DMP] solution is once again pumped through electric pump from the absorber and delivered as feed to the generators, and DE-ARS cycles continue to generate a cooling effect as shown in Fig. 1.

3. Thermodynamic analysis

The modeling and simulation to predict the performance of DE-ARS as shown in Fig. 1 using [mmim][DMP]-H_2O is established on the subsequent assumption.

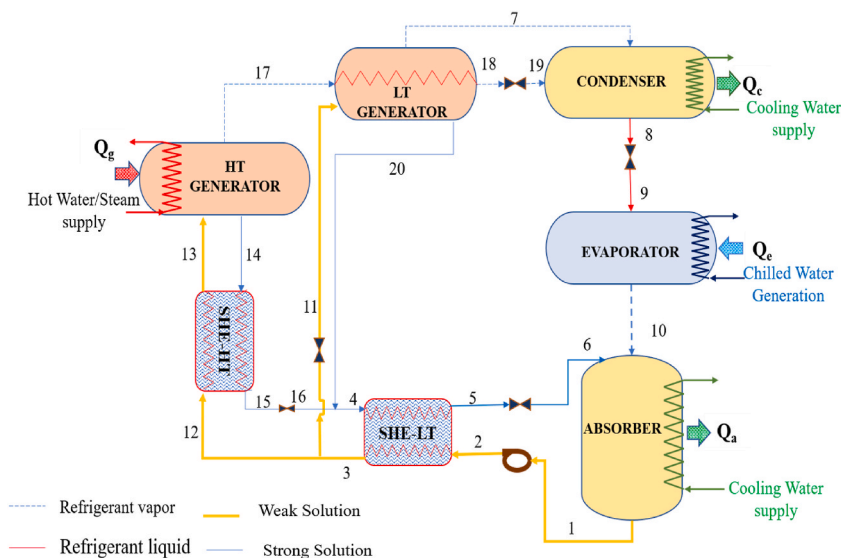- DE-ARS works in steady state environments.

Fig. 1. Double effect parallel solution flow absorption refrigeration process with two generators (HTG, LTG) and two solution heat recovery exchangers (SHE-HT, SHE-LT).

- Refrigerant leaving the condenser and evaporator is at the saturated condition.
- [mmim][DMP]-H_2O solution leaving from the bottom of the absorber, HTG and LTG are at thermodynamic equilibrium state, and this condition is used to calculate respective equilibrium composition.
- It is assumed that both the absorber and condenser temperatures are equal.
- Refrigerant water vapor flow from the HTG is constant with a mass flow rate of 1 kgs^{-1}.
- The temperature approach (ΔT_l) in LTG is assumed to constant with the value of 5K.
- Pressure drop due to friction in the ARS components and piping are assumed to be zero.
- Heat loss to ambient is zero.
- Electricity utilization of solution pumping from the absorber to generators is assumed to be the negligible and can be ignored.

3.1. Performance evaluation criteria via mass and energy balances

Thermodynamics performance analysis of DE-ARS and each subcomponent is accomplished by applying the mass conservation and energy balance (the first law of thermodynamics) for constant refrigerant flowrate of 1 kg/s from HTG consideration of previous assumptions. The general mathematical expression for the total mass balance, individual IL balance within each subcomponent of DE-ARS, mainly HTG, LTG, condenser absorber, evaporator, SHE-LT, and SHE-HT and energy balance are written under steady state conditions as follows:

$$\dot{m}_{in} - \dot{m}_{out} = 0 \tag{1}$$

$$(\dot{m}X)_{in} - (\dot{m}X)_{out} = 0 \tag{2}$$

$$(\dot{m}h)_{in} - (\dot{m}h)_{out} = 0 \tag{3}$$

Here, $\dot{m}$ is the inlet mass flow rate, X is the mass fraction of [mmim][DMP] in the [mmim][DMP]-H_2O mixture and h is the enthalpy of mixture.

DE-ARS with parallel flow consists of the distribution of weak [mmim][DMP]-H_2O solution to the LTG and HTG. The fraction of mass flowrate of the weak [mmim][DMP]-H_2O solution from the absorber is delivered to HTG as a feed called a solution distribution ratio (SDR). SDR is an important parameter and determines the performance of the DE cycle.

Overall energy balance and heat duty of subcomponent of DE-ARS mainly HTG, LTG, condenser absorber, evaporator, SHE-LT, and SHE-HT based on the first law of thermodynamics are tabulated in Table 1.

To solve the mass and energy conservation equations, a program is established in SCILAB 6.0.2. A further second SCILAB program to evaluate thermodynamics properties like Gibbs free energy, excess enthalpy, mixture enthalpy(h) of working pair [mmim][DMP]-H_2O is established. These developed models are collectively used to compute the energetic and exergetic coefficient of performance of DE-ARS as given below:

$$COP = Q_e/Q_h \tag{4}$$

$$ECOP = \frac{Q_e\left(T_{ref}/T_e - 1\right)}{Q_h\left(1 - T_{ref}/T_h\right)} \tag{5}$$

Here, exergetic COP is defined in terms of exergy or useful energy with reference-to-reference temperature. The reference temperature is a sink temperature, and which is nearly the same as ambient temperature, and therefore in this study, it is assumed that both the absorber and condenser temperatures are equal. The second law of thermodynamics deals with the concept of entropy as a physical property of the thermodynamic system and reveals the direction of spontaneous process. This governs the loss of quality of energy during the process. Exergy is the combination property of system and environment and considers both the first and second laws of

Table 1
Heat balance equation using 1st law of thermodynamics of DE-ARS for $m_{17} = 1$ kg/s.

Heat Duty of DE-ARS Component	Equation
Overall energy balance of DE-ARS	$Q_e + Q_h = Q_c + Q_a$
Evaporator	$Q_e = \dot{m}_{10}h_{10} - \dot{m}_9h_9$
Condenser	$Q_c = \dot{m}_8h_8 - \dot{m}_7h_7 - \dot{m}_{19}h_{19}$
Absorber	$Q_a = \dot{m}_{10}h_{10} + \dot{m}_6h_6 - \dot{m}_1h_1$
LTG	$Q_l = \dot{m}_{17}h_{17} + \dot{m}_{11}h_{11} - \dot{m}_7h_7 - \dot{m}_{18}h_{18} - \dot{m}_{20}h_{20}$
HTG	$Q_h = \dot{m}_{13}h_{13} - \dot{m}_{17}h_{17} + \dot{m}_{14}h_{14}$
SHE-LT	$Q_{SHEl} = \dot{m}_4(h_4 - h_5) = \dot{m}_2(h_3 - h_2)$
SHE-HT	$Q_{SHEh} = \dot{m}_{14}(h_{14} - h_{15}) = \dot{m}_{12}(h_{13} - h_{12})$

thermodynamics. Through exergy analysis, the quality of energy output of the system can be revealed. Therefore, ECOP is more meaningful than COP [54] in terms of a more complete and correct analysis.

The third parameter used to evaluate the amount of solution flowrate for pumping is the solution circulation ratio (SCR). High SCR means high solution feed to HTG in comparison to low refrigeration generator. DE-ARS is consuming a large amount of electricity for high SCR. SCR is expressed as like,

$$SCR = \dot{m}_8 \Big/ \dot{m}_1 = Solution\ Feed\ mass\ flowrate \Big/ total\ Refrigerant\ mass\ flow \tag{6}$$

$$\dot{m}_1 = \dot{m}_{17} + \dot{m}_7 \tag{7}$$

SCR is varying with the equilibrium T, P, and composition with LTG, HTG, and absorber and needs to low for efficient operation and low power consumption for pumping mixture from the absorber to the generator (low pressure to high pressure HTG and LTG). Complete program flowchart for thermodynamics analysis to obtain performances (COP, ECOP, and SCR) with the use of thermo-dynamics properties are as displayed Fig. 2. Optimum temperature and SDR to obtain maximum COP and ECOP are simulated in detail.

3.2. Thermodynamic properties

3.2.1. Water

Thermodynamics properties like enthalpy, entropy, equilibrium pressure and temperature of the refrigerant water (liquid and vapor phase) are calculated using well known IAPWS formulation and used for the performance evaluation of ARS [55].

3.2.2. Mixture $H_2O(1)$-[mmim][DMP](2)

Thermodynamics vapor-liquid equilibrium properties of H_2O-[mmim][DMP] mixture is necessary to compute enthalpy and equilibrium composition (X) within in absorber, HTG, and LTG. Excess Gibbs free energy and activity coefficient based on the NRTL model was considered to correlate mixture VLE [49]. The total vapor pressure H_2O-[mmim][DMP] mixture is equal to the partial vapor pressure of volatile refrigerant water only because ionic liquid [mmim][DMP] is nonvolatile with zero vapor pressure. The details of the excess Gibbs free energy-based NRTL model and its parameter are reported in detail by Dong et al. [49]. Here NRTL model fitting parameters are directly used to evaluate the enthalpy of H_2O-[mmim][DMP] mixture using excess Gibbs free energy(g^E). The excess enthalpy (h^E) using g^E is as given below,
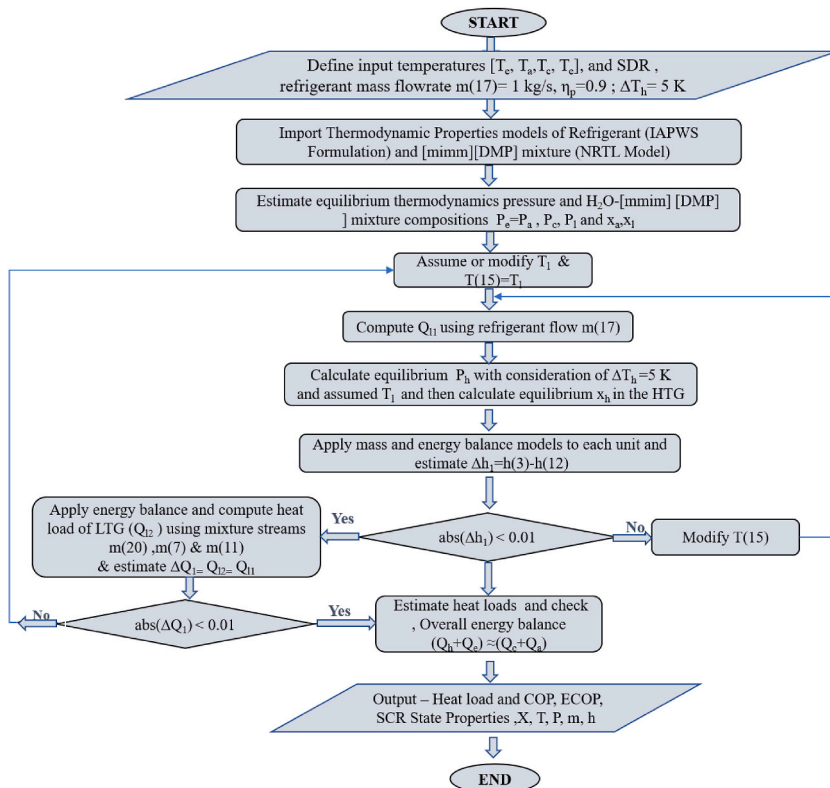

Fig. 2. Performance evaluation modeling and simulation flowchart of DE-ARS using H_2O-[mmim][DMP] mixture.

$$h = x_1 h_1 + x_2 h_2 + h^E \tag{8}$$

where,

$$h^E = - RT^2 \left[\frac{d(g^E/RT)}{dT} \right]_P \tag{9}$$

Where, x is the molar composition of each component in the H_2O-[mmim][DMP] solution, h_1 is the enthalpy of liquid refrigerant H_2O at saturated condition, h_2 is the enthalpy of IL [mmim][DMP] at the pure state. h_2 is calculated from the heat capacity (Cp_2) of pure [mmim][DMP] and temperature difference [56].

4. Result and discussion

4.1. Validation of thermodynamics property of H₂O-[mmim][DMP] mixture

At first, the verification of thermodynamic properties of H_2O-[mmim][DMP] mixture with the published literature is essential for the detailed performance study of DE-ARS. Separate SCILAB mathematical computer programs for the calculation of thermodynamics properties of the proposed H_2O-[mmim][DMP] mixture and pure water are developed. These programs have been employed as input module to the subsequent SCILAB program related to modeling and simulation of single effect ARS. Accordingly, the thermodynamic properties of the proposed [mmim][DMP]-H_2O mixture and performance of single effect ARS is verified with Dong et al. and Takalkar and Sleiti [49,50]. Performance comparison of the COP plots have revealed good agreement for the generator temperature range of 63–120°C. This validates the modeling and simulation approach resulted to predict the thermodynamics properties of proposed H_2O-[mmim][DMP] mixture and employed thermodynamic nonrandom two liquid model based activity coefficient modal.

4.2. Validation of DE-ARS (parallel flow) models using H₂O-[mmim][DMP] mixture

Further to verify the mathematical models of parallel flow DE-ARS using H_2O-[mmim] [DMP] mixture, simulation of conventional H_2O–LiBr mixture are performed for temperatures $T_e/T_h/T_a/T_c$ of 5/115/30/30°C and 4/134/35/35°C. For this, we developed an independent computer program in SCILAB to assess the thermodynamics properties of the H_2O–LiBr solution [57] and the performance of DE-ARS using H_2O–LiBr mixture [46,58]. Performance simulation are compared with the published data as described in Table 2. It can be seen that, COP of DE-ARS for $T_e/T_h/T_a/T_c$ of 5/115/30/30°C and 4/134/35/35°C demonstrates good agreement with the Bagheri et al. and Azhar et al. [13,59]. Further, the performance of DE-ARS using H_2O–LiBr is compared with the proposed H_2O-[mmim][DMP] mixture for $T_e/T_h/T_a/T_c$ of 5/140/30/30°C. Tabulated data 3 reveals the detailed thermodynamic properties (like T, P, X_2, h, m) of each process stream of H_2O–LiBr and H_2O-[mmim][DMP] mixture driven DE-ARS for $T_e/T_h/T_a/T_c$ of 5/140/30/30°C. The simulated COP and ECOP of H_2O-[mmim][DMP] driven DE-ARS were found to be higher than H_2O–LiBr by 5.22% and 4.95%, respectively. In terms of SCR, H_2O–LiBr mixture demonstrated lowered value of 7.81, which is nearly half of the SCR of H_2O-[mmim] [DMP] mixture. It means, H_2O-[mmim][DMP] mixture expend high pumping power to drive the weak solution from the absorber to HTG and LTG to fulfil the same cooling capacity. Further, to compare and evaluate the definite difference between two working pairs, a detailed comparison was performed in the next subsection (see Table 3).

4.3. Comparison of LiBr–H₂O and H₂O-[mmim][DMP] mixture

Fig. 3 depicts the effect of HTG temperature on the performances of DE-ARS namely COP, ECOP, SCR, and heat load distribution fraction in between LTG and HTG (Q_l/Q_h) at constant evaporation temperature of 5°C, absorption and condensation temperatures of 30°C. As noticed in Fig. 3a/b, both COP and ECOP of working fluids with the upsurge in T_h start to increase at first, achieve maxima, and then finally begin to diminish. An optimum T_h to achieve maximum COP is found to be higher than optimum T_h based on

Table 2
Model validation of DE refrigeration cycle by considering H_2O–LiBr and H_2O-[mmim] [DMP] as a working pair.

Parameter	Bagheri et al. [59] - H_2O–LiBr	Present Simulation- H_2O–LiBr	Azhar and Altamush [13] - H_2O–LiBr	Present Simulation- H_2O–LiBr	Present Simulation H_2O-mmim [DMP]
T_e	4	4	5	5	5
T_h	134	134	115	115	115
$T_a=T_c$	35	35	30	30	30
ε_{SHE}	0.7	0.7	0.7	0.7	0.7
SDR	0.36	0.36	0.5	0.5	0.5
dT_l	10	10		5	5
COP	1.129	1.120	1.401	1.406	1.22
ECOP		0.515		0.561	0.5
SCR		24.538		13.26	25.94

Table 3

Comparison of Simulation conventional H_2O–LiBr and proposed H_2O-mmim [DMP]working pair for SDR = 0.33; $\varepsilon_{SHE} = 0.9$; $\Delta T_l = 5$ K.

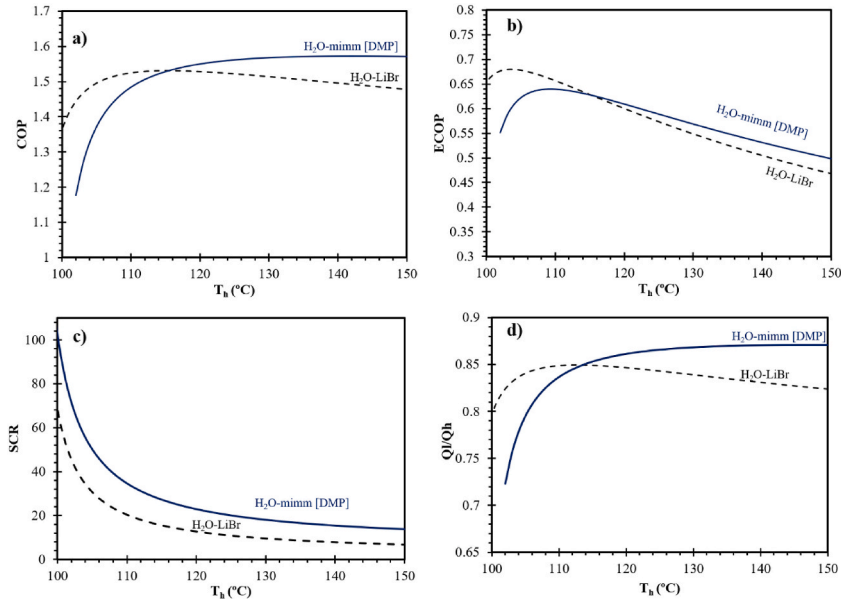| Stream Number	$H_2O(1)$–LiBr(2)					$H_2O(1)$-[mmim][DMP](2)				
	$T/°C$	P /kPa	X_2	h /(J·g⁻¹)	$\dot{m}$ /(kg·s⁻¹)	$T/°C$	P /kPa	X_2	h /(J·g⁻¹)	$\dot{m}$ /(kg·s⁻¹)
1	30	0.87	0.53	66.63	14.46	30	0.87	0.82	22.93	29.84
2	30	36.35	0.53	66.63	14.46	30	33.20	0.82	22.93	29.84
3	57.95	36.35	0.53	125.49	14.46	60.06	33.20	0.82	88.90	29.84
4	69.66	4.25	0.60	175.95	12.61	67.03	4.25	0.88	104.01	27.98
5	33.97	4.25	0.60	108.44	12.61	33.70	4.25	0.88	33.64	27.98
6	33.97	0.87	0.60	108.44	12.61	33.70	0.87	0.88	33.64	27.98
7	68.58	4.25	0	2,628.66	0.85	66.44	4.25	0	2,624.63	0.87
8	30	4.25	0	125.75	1.85	30	4.25	0	125.75	1.87
9	5	0.87	0	125.75	1.85	5	0.87	0	125.75	1.87
10	5	0.87	0	2,510.07	1.85	5	0.87	0	2,510.07	1.87
11	57.95	4.25	0.53	125.50	9.64	60.06	4.25	0.82	88.89	19.90
12	57.95	36.35	0.53	125.50	4.82	60.06	33.20	0.82	88.89	9.95
13	105.54	36.35	0.53	229.17	4.82	123.95	33.20	0.82	262.27	9.95
14	140	36.35	0.66	339.17	3.82	140	33.20	0.92	299.08	8.95
15	66.16	36.35	0.66	208.36	3.82	68.06	33.20	0.92	106.33	8.95
16	66.16	4.25	0.66	208.36	3.82	68.06	4.25	0.92	106.33	8.95
17	140	36.35	0	2,761.79	1	140	33.20	0	2,762.03	1
18	73.58	36.35	0	308.00	1	71.44	33.20	0	299.05	1
19	73.58	4.25	0	308.00	1	71.44	4.25	0	299.05	1
20	68.58	4.25	0.58	161.87	8.79	66.44	4.25	0.86	102.92	19.03
COP	1.495					1.573				
ECOP	0.505					0.53				
SCR	7.81					15.99				
Q_h/Q_l	1.20					1.15				

Fig. 3. Variation of COP, ECOP, SCR, and Ql/Qh of DE-ARS parallel flow with an increase in T_h for H_2O–LiBr and H_2O-[mmim][DMP] for constant SDR = 0.33, $T_e = 5°C$ $T_a = T_c = 30°C$, SDR = 0.33.

maximum ECOP. In the case of H_2O–LiBr mixture, an optimum T_h based on COP and ECOP is $112°C$ and $105°C$ respectively. Compared to H_2O–LiBr, COP, and ECOP of H_2O-[mmim][DMP] mixture begin to become better for generator temperature more than $115°C$. This signifies that, H_2O–LiBr mixture is better to utilize a low-temperature heat source below $115°C$. However, a high-temperature heat source (more than $115°C$) to DE-ARS is preferred to generate better performance for H_2O-[mmim][DMP] mixture. This is mainly due to the optimization of equilibrium mixture composition within HTG and LTG and maximum utilization of heat energy as observed in Fig. 3d. Fig. 3c reveals the variation of SCR with T_h wherein SCR of H_2O–LiBr mixture is continuously lower than the SCR of H_2O-[mmim][DMP] mixture due to difference in equilibrium composition of absorbent inside the absorber and generator.

Working fluid comparison and effect of T_e, T_a and T_c on the COP of parallel flow DE-ARS for $T_e/T_c/T_a$ of 10/30/30°C, 10/40/40°C and 5/30/30°C is revealed in Fig. 4. Overall, high evaporation temperature and low temperature of absorption and condensation enhances performance of DE-ARS due to the improved refrigerant vapor absorption rate at high evaporation pressure and low absorber temperature. Such enhanced water vapor absorption into the incoming strong solution generates a weaker solution inside the absorber of DE-ARS. Enhanced water vapor absorption boosts the equilibrium concentration difference between strong and weak mixture. Further as seen in Fig. 4, DE-ARS utilizes low-temperature heat more efficiently for input temperature $T_e/T_c/T_a$ of 10/30/30°C than 10/40/40°C and 5/30/30°C. As discussed previously, compared to H_2O-[mmim] [DMP] mixture, COP of H_2O–LiBr mixture was found to be low at high T_h. It can be viewed that on large, the low sink temperature (T_a=T_c) and high evaporation temperature produce better COP for H_2O-[mmim][DMP] than H_2O–LiBr mixture.

4.4. Sensitivity analysis

4.4.1. Effect of solution distribution ratio (SDR)

The effect of solution distribution ratio on the performance parameters of DE-ARS like COP, ECOP, and SCR are exhibited in Fig. 5. COP of DE-ARS initially increases with the rise in SDR then achieves maxima and at the end COP starts to decline very slow rate., COP approximately becomes constant over SDR of 0.3 for which half of the weak solution flowed from the absorber to HTG. Also, at constant SDR, COP of T_h of 140°C are found to be better than $T_h = 100°C$ due to the high concentration of strong H_2O-[mmim][DMP] solution leaving from the generators. Such a high difference in equilibrium concentration of weak and strong H_2O-[mmim][DMP] solution improves the efficiency of DE-ARS. As like COP trend, a similar performance variation is noted for exergy-based performance. However, ECOP variation is less for HTG temperature of 140°C than 110°C due to high exergy loss.

Fig. 6 shows the effect of HTG temperature and SDR on COP, ECOP, SCR, and Q_l/Q_h (heat load fraction of low to high-temperature generator) for $T_e = 5°C$, $T_a/T_c = 30°C$. COP and ECOP variation depict better performances for the high value of SDR. The major difference in both performances of DE-ARS is viewed for SDR in the range of 0.1–0.3. SDR greater than 0.3 reveals a marginal variation in the COP and ECOP. Further at higher T_h, COP starts to diminish with rising SDR from 0.3 to 0.5. For example, at $T_h = 140°C$, SDR of 0.1 showed the lowest COP and ECOP of 1.49 and 0.5; then performances (COP and ECOP) improved till SDR of 0.3 with values of 1.57 and 0.53, respectively. Afterwards (SDR more than 0.3), COP start to decrease at a slower rate till SDR of 0.5 with COP of 1.56 and ECOP of 0.52. In the current simulation study a maximum COP of 1.57 was achieved for the SDR of 0.3 and T_h of 150°C, and the maximum ECOP of 0.638 was attained for SDR of 0.4 with T_h of 109°C.

The minimum temperature of HTG at which DE-ARS start to become feasible to produce a cooling effect and reveal lowest COP and ECOP is slashed with the rise in SDR from 0.1 to 0.3 and then nearly become constant till SDR of 0.5. This indicates that the utilization of low-temperature solar heat to produce cooling effect is improved after SDR greater than 0.3. At SDR of 0.5, COP of DE-ARS improves with the increase in temperature of HTG and achieves a maximum and then starts to decrease at a slower rate.

SCR plot reveals decline with the rise in both T_h and SDR. At higher T_h (likely more than 120°C) with SDR greater than 0.3, the rate of SCR reduction becomes almost flat. This means at higher T_h, and SDR of 0.3, 0.4, and 0.5, the power required to pump the weak solution is approximately same. Further, Q_l/Q_h variation was found to improve with the rise in T_h but it reduces with the increase in SDR from 0.1 to 0.5. High T_h inside HTG generates the high temperature H_2O vapor with reduction in equilibrium concentration of strong H_2O-[mmim][DMP] mixture in HTG. Overall, produced high-temperature water vapor within HTG is distributed as a feed and heat source to LTG; this upsurges in solution temperature within LTG, ultimately increasing the equilibrium concentration of H_2O-[mmim][DMP] mixture and generates more refrigerant H_2O vapor.

4.4.2. Effect of evaporation temperature

The impact of evaporation temperature on the COP, ECOP, and SCR for T_e of 5, 10, and 15°C are as displayed in Fig. 7. It clearly indicates the high evaporation temperature of DE-ARS provides better COP (Fig. 7a) and ECOP ((Fig. 7b) due to high equilibrium
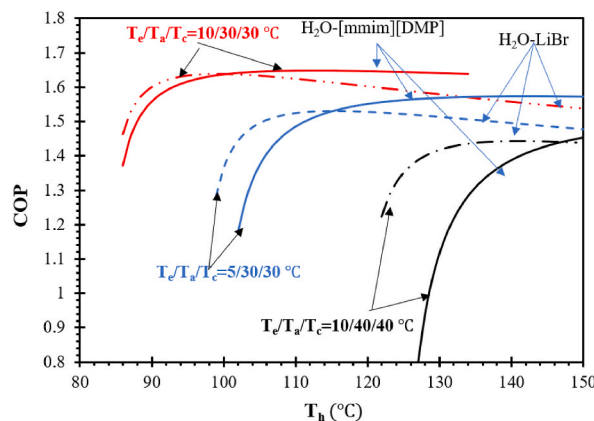

Fig. 4. Comparison of COP of H_2O-[mmim][DMP] driven DE ARS with H_2O–LiBr for $T_e/T_a/T_c$ of 10/30/30°C, 5/30/30°C, 10/40/40°C
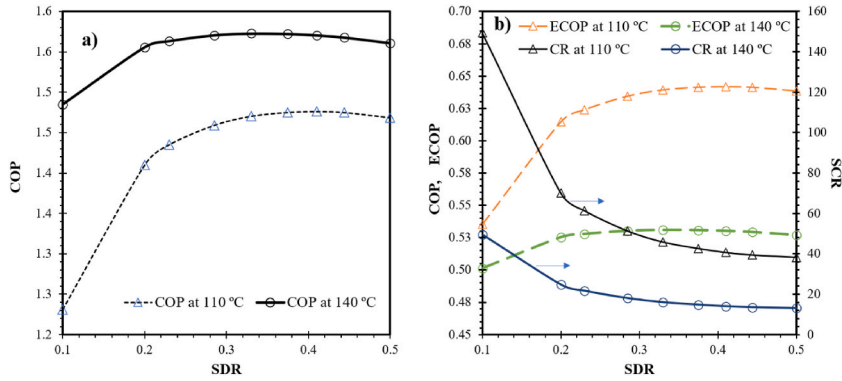
Fig. 5. Effect solution distribution from the absorber to HTG and LTG at T_h of $140°C$ and $110°C$ with $T_e/T_c/T_a$ of $5/30/30°C$
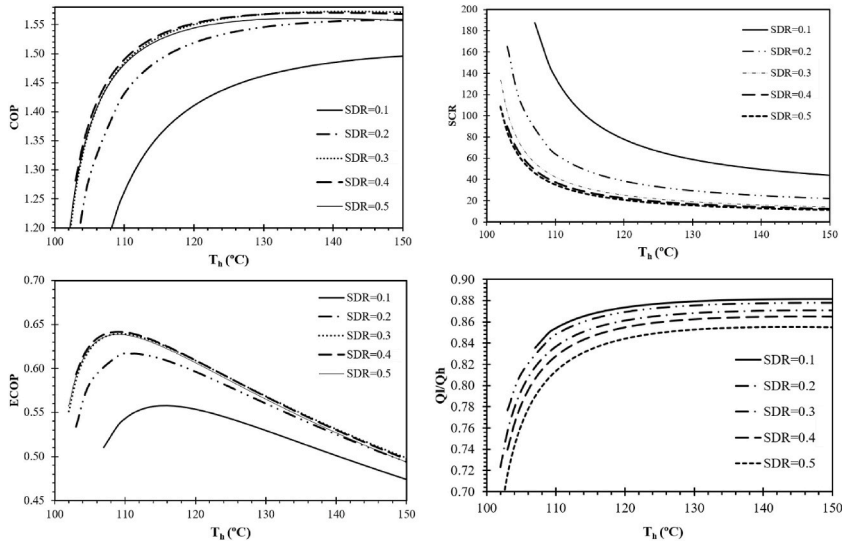

Fig. 6. Effect of HTG temperature and SDR on COP. ECOP, SCR and Ql/Qh for $T_a/T_c = 30°C$, $T_e = 5°C$

pressure within absorber and evaporator. High evaporation pressure boosts the water vapor absorption capacity into the strong solution of H_2O-[mmim][DMP] mixture. As displayed in Fig. 7d, the equilibrium composition difference between weak (X_a) and strong solutions within HTG and LTG (X_h and X_l) becomes more with the rise in T_e from 5 to $15°C$. Such Improved concentration gradient at high T_e reduces the solution circulation rate as seen in Fig. 7c. As a case T_h of $110°C$, the composition difference between weak and strong solution is noticed to be high for T_e of $15°C$, and then it reduces with the reduction in T_e to $5°C$. Likewise, within investigated evaporation temperature, T_e of $15°C$ revealed lowest SCR of 11 for T_h of $110°C$, which is 75% lowered than T_e of $5°C$. Solution pumping power required to flow weak solution for high Te of $15°C$ is lower due to low SCR.

4.4.3. Effect of absorber and condenser temperature

The temperature of the absorber (T_a) and condenser (T_c) is determined by the ambient or sink temperature since the heat of absorption and condensation is dissipated to ambient either water cooled and air-cooled heat transfer system, respectively. Low T_a and T_c improve the heat transfer rate with the increase in temperature gradient. Therefore, effect of T_a and T_c on the performance of DE-ARS is vital to investigate in detail. The detailed performance simulation is presented in Fig. 8 for three $T_a = T_c$ of 30, 35, and $40°C$.

It is clear that lower value of T_a and T_c is more beneficial to enhance both energetic COP (Fig. 8a) and exergetic COP (Fig. 8a). Further, low sink temperature is beneficial to utilize low-grade heat more efficiently within the HTG of DE-ARS. The main reason to boost the cyclic performance at low T_a is enhanced to water vapor absorption capacity into the strong H_2O-[mmim][DMP] mixture. Ultimately this enhanced absorption at low T_a declines the equilibrium concentration of [mmim][DMP] in the absorber. Overall, the combined effect of low T_a and T_c diminishes SCR (Fig. 8c) of DE-ARS and which ultimately diminishes pumping power. Drop in T_c from 40 to $30°C$ diminishes the saturation pressure of refrigerant water vapor condensation within condenser and pressure of LTG as manifested in Fig. 8d. Such low T_c and saturation pressure is very useful for efficient consumption of low-grade heat within DE-ARS to generate cooling. Further low T_c reduces the pressure of water vapor condensation within condenser and supplied heat temperature of
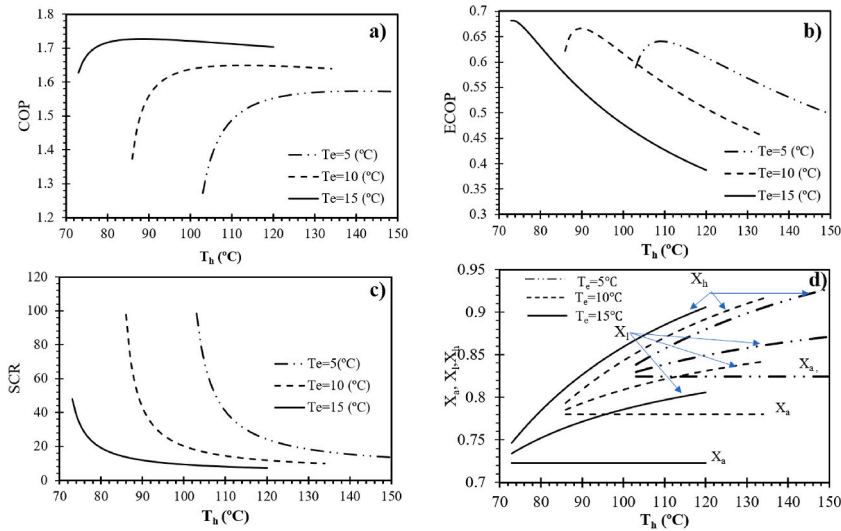
Fig. 7. Effect of temperature of refrigerant evaporation on a) COP, b) Exergetic COP, c) SC and d) equilibrium concentration within absorber (X_a), LTG (X_l) and HTG(X_h) of parallel flow DE-ARS using H_2O-[mmim][DMP] binary mixture for SDR = 0.33 and $T_a = T_c = 30°C$
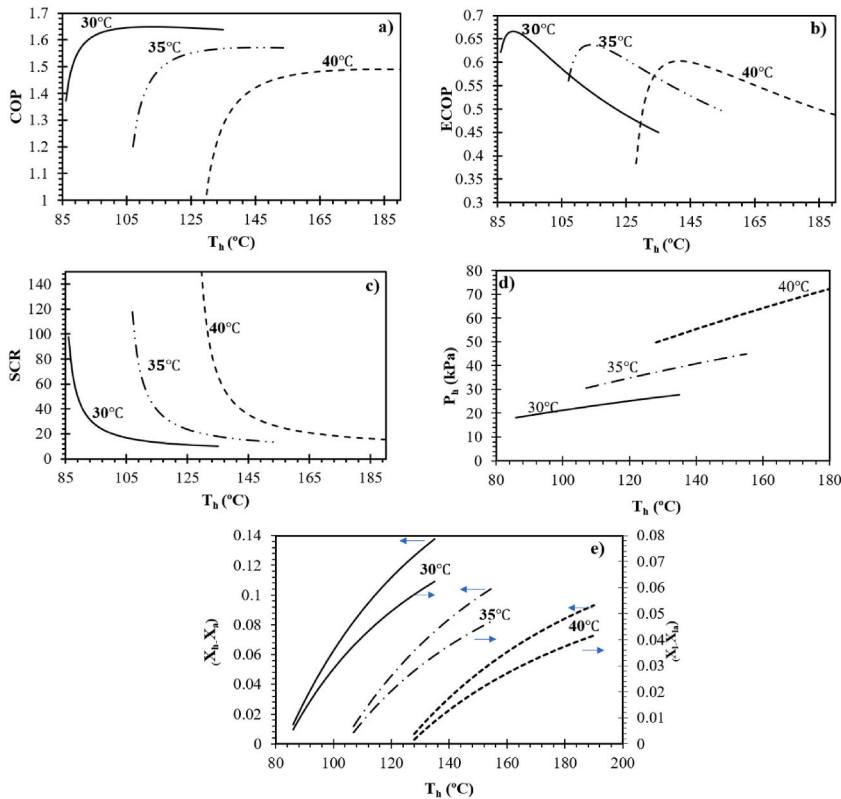

Fig. 8. Effect of sink temperature in term of $T_a = T_c$ on a) COP, b) ECOP, c) SCR d) P_h, and e) equilibrium concentration gradient (X_h-X_a), (X_l-X_a) of parallel flow DE-ARS of H_2O-[mmim][DMP] binary mixture for SDR = 0.33, $T_e = 10°C$

HTG. Equilibrium concentration difference of H_2O-[mmim][DMP] mixture between LTG and HTG expands vastly with the reduction in T_a and T_c as depicted in Fig. 8e. Overall, the combined effect of low T_a and T_c diminishes SCR (Fig. 8c) of DE-ARS and which ultimately diminishes pumping power.

4.5. Performance optimization and comparison

A previous study reveals the impact of evaporation temperature, condensation temperature, and absorber temperature on the efficiency parameters of DE-ARS. Optimum performances towards utilization of low-grade heat more efficiently within the generator of DE-ARS is essential to compute over a wide range of T_e, T_a, and T_c. Table 4 shows the simulation results to predict optimum performances of studied working binary mixture H_2O-[mmim][DMP] and further it shows the comparison with the commercial working fluid H_2O–LiBr. The performance optimization study covers a broad range of evaporation temperature from 5 to $20°C$.

From the tabulated data at $T_e = 5°C$, an optimum T_h to achieve COP_{max} using H_2O–LiBr driven DE-ARS is boosted from $114°C$ to $154°C$, but COP_{max} reduces from 1.53 to 1.38 as $T_a{=}T_c$ increase from 30 to $40°C$ respectivley. For a similar case with $T_e = 5°C$, an optimum T_h of H_2O-[mmim][DMP] mixture driven DE-ARS rises from $141°C$ to $208°C$ with the decline in COP_{max} from 1.57 to 1.4 with the rise in $T_a{=}T_c$ from 30 to $40°C$. This indicates that H_2O-[mmim][DMP] mixture gives high COP_{max} for high-temperature heat source and alternatively H_2O–LiBr driven ARS delivers better COP_{max} for the utilization of low-temperature heat source.

COP comparison between H_2O–LiBr and H_2O-[mmim][DMP] mixture for same T_h is also simulated wherein T_h is selected correspond to COP_{max} of H_2O–LiBr. The simulation results show that the COP of H_2O-[mmim][DMP] mixture approximately equal to COP_{max} of H_2O–LiBr. As a case T_e of $20°C$, COP of H_2O–LiBr and H_2O-[mmim][DMP] is 1.64 and 1.638 respectively at the same HTG temperature of $110°C$.

Further $ECOP_{max}$ of DE-ARS using H_2O-[mmim][DMP] mixture reduces from 0.64 to 0.57 with the increase in T_h from $109°C$ to $169°C$. Energy and exergy-based performance comparison showed that optimum T_h based on $ECOP_{max}$ is found to be lower than COP_{max}. Overall, the simulation results show uppermost COP_{max} and $ECOP_{max}$ of 1.81 and 0.69 for T_e of $20°C$ and $T_a{=}T_c{=}30°C$. Also, for these operating condition ($T_e = 20°C$ and $T_a{=}T_c{=}30°C$), DE-ARS requires low-temperature heat of 68 and $60°C$ to achieve maximum COP and ECOP, respectively. Such T_h is lower than the optimum T_h ($72°C$) of LiBr–H_2O driven DE-ARS. Therefore, in general COP and ECOP of DE-ARS enhances with the rise in evaporation temperature and decline in absorber and condenser temperature.

5. Conclusions

The utilization of solar energy for heating, cooling and refrigeration is an attractive green approach to reduce CO_2 emissions that can lessen peak demand of high-grade energy during summer. Solar powered absorption refrigeration system for upcoming and developing cities can be more attractive during high solar radiation time in hot arid countries to fulfill the cooling demand. The centralized solar thermal powered vapor absorption refrigeration and cooling systems can significantly lower greenhouse effect with the large reduction in electricity consumption.

Accordingly, in this study, a parallel flow double effect absorption refrigeration system due to efficient utilization of low-temperature heat below $200°C$ was investigated using ionic liquid based H_2O-[mmim][DMP] binary solution as a potential alternative working pair to conventional H_2O–LiBr. The thermodynamics properties of novel H_2O-[mmim] [DMP] working mixture were computed by considering the local composition based NRTL model. The thermodynamics properties of H_2O-[mmim] [DMP] mixture and refrigerant H_2O were computed and verified with the modeling and simulation of single effect ARS for $T_e/T_c/T_a$ of 10/40/30 °C. The performance of DE-ARS was validated with the conventional LiBr–H_2O for temperatures $T_e/T_h/T_a/T_c$ of 5/115/30/30 °C and 4/134/35/35 °C. Simulated COP in both cases showed good agreement with the published literature and validate thermodynamic properties of proposed mixture. The energy and exergy performance of DE-ARS was assessed for a wide range of T_e, T_h, T_a and T_c. Simulation results in comparison of H_2O-[mmim] [DMP] mixture with conventional H_2O–LiBr mixture indicates that.

- High T_h generates higher COP but lower ECOP of DE-ARS for H_2O-[mmim][DMP] mixture.

Table 4
Optimization and comparison of the performance of H_2O-[mmim][DMP] with commercial working pair H_2O–LiBr for T_e of 5, 10, 15, $20°C$ and $T_a{=}T_c{=}30,35,40°C$ with SDR of 0.35.

T_e ($°C$)	$T_a{=}T_c$ ($°C$)	H_2O–LiBr[46]			H_2O-[mmim][DMP]				
		COP	Optimum T_h ($°C$)	T_{hmin}	COP_{max}	Optimum T_h ($°C$)	$ECOP_{max}$	Optimum T_h ($°C$)	COP based on optimum T_h of H_2O/LiBr-
5	30	1.53	114	103	1.57	141	0.64	109	1.524
	35	1.44	134	124	1.49	179	0.60	137	1.36
	40	1.38	154	148	1.4	208	0.57	169	1.05
10	30	1.63	100	86	1.65	114	0.67	90	1.64
	35	1.53	119	107	1.57	145	0.64	114	1.524
	40	1.45	138	128	1.49	183	0.60	141	1.346
15	30	1.73	86	73	1.73	89	0.68	73	1.73
	35	1.63	105	91	1.65	118	0.66	95	1.64
	40	1.54	124	111	1.57	150	0.64	119	1.52
20	30	1.82	72	60	1.81	68	0.69	60	1.805
	35	1.73	91	78	1.73	94	0.68	78	1.727
	40	1.64	110	96	1.65	120	0.66	100	1.638

- Low-temperature heat utilization of H_2O–LiBr mixture showed better COP at high sink temperature of T_a/T_c of 40 °C.
- SCR of H_2O–LiBr mixture was found to be lower than H_2O-[mmim][DMP] mixture.
- H_2O-[mmim][DMP] mixture demonstrated lower COP and ECOP of 1.22 and 0.5 for $T_e/T_h/T_a/T_c$ of 5/115/30/30 °C.

Some of the main conclusions of sensitivity analyses and optimization of proposed H_2O-[mmim][DMP] driven parallel flow DE-ARS are as given below.

- COP and ECOP of DE-ARS were found to be increasing with SDR till 0.3 and then gave nearly similar range COP, however SCR is decreased with rising in SDR and becomes almost the same after SDR of 0.3.
- Effect T_e and T_a/T_c on the performances of H_2O-[mmim][DMP] mixture revealed improved COP and ECOP for high T_e and low T_a/T_c due to variation of equilibrium pressure and composition within in HTG, LTG, and absorber.
- Optimization results based on T_e from 5 to 20°C and T_a/T_c from 30 to 40°C showed that maximum COP of 1.81 for $T_e/T_a/T_c/T_h$ of 20/30/30/68°C.

In general, examined H2O-[mmim][DMP] mixture showed benefits to improve the energy performance of DE-ARS and to overcome the drawback of conventional H2O–LiBr mixture. High-temperature heat is efficiently utilized by H_2O-[mmim][DMP] mixture driven parallel flow DE-ARS, and it gives basic criteria for the selection of H_2O-[mmim][DMP] mixture for the replacement of conventional working mixture for cooling purposes. The feasibility of the H_2O-[mmim][DMP] mixture for different multistage cycle configurations and to utilize low-grade heat more efficiently is under investigation of future study.

Author statement

M. Salim Ferwati: Writing original draft, Investigation, Project administration, Funding acquisition, Supervision Ahmad Mohammad Ahmad: Investigation, Data Curation, Visualization, writing– review & editing. Gorakshnath Dadabhau Takalkar: Conceptualization, Methodology, Software, Validation, Formal analysis, Supervision, writing – review & editing Yusuf Bicer: Investigation, Data Curation, Writing – review & editing.

Declaration of competing interest

The authors declare that they have no known competing financial interests or personal relationships that could have appeared to influence the work reported in this paper.

Acknowledgements

Nomenclature

Variables

C_P	heat capacity, *kJ/kgK*
g	Gibbs energy
h	Enthalpy, *kJ/kg*
$\dot{m}$	Mass flow rate, *kg/s*
P	Total pressure, *kPa*
Q	Heat load, *kW*
R	Gas constant, *kJ/(kmol K)*
T	Temperature°*C*
X_2	Mass fraction of absorbent into a binary mixture
x_1	mole fraction of refrigerant into a binary mixture

Subscripts

1,2,3	state points
a	Absorber
c	Condenser
E	excess
e	Evaporator
g	Generator
h	High temperature generator
l	Low temperature generator
ref	reference

max   Maximum

Abbreviations

ARS   Absorption refrigeration system
COP   Coefficient of performance
DE-ARS   Double effects absorption refrigeration system
ECOP   Exergetic Coefficient of performance
HTG   High temperature generator
LTG   Low temperature generator
LiBr   Lithium bromide
[mmim][DMP] 1,3-dimethylimidazolylium dimethylphosphate
SCR   Solution circulation ratio
SDR   Solution distribution ratio
SE-ARS   Single effect Absorption refrigeration system
SHE-LT   Solution heat exchange low temperature
SHE-HT   Solution heat exchange high temperature

References

[1] S.S. Alrwashdeh, H. Ammari, Life cycle cost analysis of two different refrigeration systems powered by solar energy, Case Stud. Therm. Eng. 16 (2019), https://doi.org/10.1016/j.csite.2019.100559.

[2] S.M. Babaei, A.R. Razmi, M. Soltani, J. Nathwani, Quantifying the effect of nanoparticles addition to a hybrid absorption/recompression refrigeration cycle, J. Clean. Prod. 260 (2020), 121084, https://doi.org/10.1016/j.jclepro.2020.121084.

[3] D. Perez-Astudillo, D. Bachour, DNI, GHI and DHI ground measurements in Doha, Qatar, Energy Procedia 49 (2013) 2398–2404, https://doi.org/10.1016/j.egypro.2014.03.254.

[4] D. Bachour, D. Perez-Astudillo, Ground-measurement GHI map for Qatar, Energy Procedia 49 (2013) 2297–2302, https://doi.org/10.1016/j.egypro.2014.03.243.

[5] V. Eveloy, D.S. Ayou, Sustainable district cooling systems: status, challenges, and future opportunities, with emphasis on cooling-dominated regions, Energies 12 (2019), https://doi.org/10.3390/en12020235.

[6] D.F. Dominković, K.A. Bin Abdul Rashid, A. Romagnoli, A.S. Pedersen, K.C. Leong, G. Krajačić, N. Duić, Potential of district cooling in hot and humid climates, Appl. Energy. 208 (2017) 49–61, https://doi.org/10.1016/j.apenergy.2017.09.052.

[7] A. Al-Falahi, F. Alobaid, B. Epple, Design and thermo-economic comparisons of large scale solar absorption air conditioning cycles, Case Stud. Therm. Eng. 22 (2020), https://doi.org/10.1016/j.csite.2020.100763.

[8] D.M. Alghool, T.Y. Elmekkawy, M. Haouari, A. Elomri, Optimization of design and operation of solar assisted district cooling systems, Energy Convers. Manag. X. 6 (2020), 100028, https://doi.org/10.1016/j.ecmx.2019.100028.

[9] I. Sarbu, C. Sebarchievici, Review of solar refrigeration and cooling systems, Energy Build 67 (2013) 286–297, https://doi.org/10.1016/j.enbuild.2013.08.022.

[10] C. Tzivanidis, E. Bellos, The use of parabolic trough collectors for solar cooling - a case study for Athens climate, Case Stud. Therm. Eng. 8 (2016) 403–413, https://doi.org/10.1016/j.csite.2016.10.003.

[11] P. Soto, L.A. Domínguez-Inzunza, W. Rivera, Preliminary assessment of a solar absorption air conditioning pilot plant, Case Stud. Therm. Eng. 12 (2018) 672–676, https://doi.org/10.1016/j.csite.2018.09.001.

[12] O. Rejeb, C. Ghenai, M. Bettayeb, Modeling and simulation analysis of solar absorption chiller driven by nanofluid-based parabolic trough collectors (PTC) under hot climatic conditions, Case Stud. Therm. Eng. 19 (2020), https://doi.org/10.1016/j.csite.2020.100624.

[13] M. Azhar, M. Altamush Siddiqui, Comprehensive exergy analysis and optimization of operating parameters for double effect parallel flow absorption refrigeration Cycle, Therm. Sci. Eng. Prog. 16 (2020), 100464, https://doi.org/10.1016/j.tsep.2019.100464.

[14] X. Zheng, R. Shi, Y. Wang, S. You, H. Zhang, J. Xia, S. Wei, Mathematical modeling and performance analysis of an integrated solar heating and cooling system driven by parabolic trough collector and double-effect absorption chiller, Energy Build 202 (2019), 109400, https://doi.org/10.1016/j.enbuild.2019.109400.

[15] S.F. Mussati, S.S. Mansouri, K.V. Gernaey, T. Morosuk, M.C. Mussati, Model-based cost optimization of double-effect water-lithium bromide absorption refrigeration systems, Processes 7 (2019), https://doi.org/10.3390/pr7010050.

[16] X. Sun, L. Liu, Y. Zhuang, L. Zhang, J. Du, Heat exchanger network synthesis integrated with compression-absorption cascade refrigeration system, Processes 8 (2020), https://doi.org/10.3390/pr8020210.

[17] S. Sharifi, F. Nozad Heravi, R. Shirmohammadi, R. Ghasempour, F. Petrakopoulou, L.M. Romeo, Comprehensive thermodynamic and operational optimization of a solar-assisted LiBr/water absorption refrigeration system, Energy Reports 6 (2020) 2309–2323, https://doi.org/10.1016/j.egyr.2020.08.013.

[18] A. Allouhi, T. Kousksou, A. Jamil, P. Bruel, Y. Mourad, Y. Zeraouli, Solar driven cooling systems: an updated review, Renew. Sustain. Energy Rev. 44 (2015) 159–181, https://doi.org/10.1016/j.rser.2014.12.014.

[19] X. Yan, Y. Shi, N. Gao, G. Chen, Experimental investigation on a novel triple heat sources-driven absorption heat pump system, Energy Build 198 (2019) 28–37, https://doi.org/10.1016/j.enbuild.2019.05.058.

[20] K. Mohammadi, M. Saghafifar, J.G. McGowan, K. Powell, Thermo-economic analysis of a novel hybrid multigeneration system based on an integrated triple effect refrigeration system for production of power and refrigeration, J. Clean. Prod. 238 (2019), https://doi.org/10.1016/j.jclepro.2019.117912.

[21] P. Reza, Shirmohammadi Alireza, Aslani Roghayeh, M. Ghasempour Luis, Romeo Fontina, Process design and thermoeconomic evaluation of a CO2 liquefaction process driven by waste exhaust heat recovery for an industrial CO2 capture and utilization plant, J. Therm. Anal. Calorim. 145 (2021) 1585–1597. https://link.springer.com/article/10.1007/s10973-021-10833-z.

[22] L.M. Shirmohammadi, R. Soltanieh, M. Romeo, Thermoeconomic analysis and optimization of post-combustion CO2 recovery unit utilizing absorption refrigeration system for a natural-gas-fired power plant, Environ. Prog. Sustain. Energy. 37 (2018) 1075–1084, https://doi.org/10.1002/ep.12866.

[23] Z. Long, Y. Luo, H. Li, X. Bu, W. Ma, Performance analysis of a diffusion absorption refrigeration cycle working with TFE-TEGDME mixture, Energy Build 58 (2013) 86–92, https://doi.org/10.1016/j.enbuild.2012.12.003.

[24] W. Wu, B. Wang, T. You, J. Wang, W. Shi, X. Li, Compression-assisted absorption cycles using ammonia and various ionic liquids for cleaner heating, J. Clean. Prod. 195 (2018) 890–907, https://doi.org/10.1016/j.jclepro.2018.05.270.

[25] D. Zheng, L. Dong, W. Huang, X. Wu, N. Nie, A review of imidazolium ionic liquids research and development towards working pair of absorption cycle, Renew. Sustain. Energy Rev. 37 (2014) 47–68, https://doi.org/10.1016/j.rser.2014.04.046.

[26] K. Li, W. Wu, J. Wu, H. Liang, H. Zhang, Experiments on vapour-liquid equilibrium of CO2-ionic liquid under flow conditions and influence on its refrigeration cycle, Appl. Therm. Eng. 180 (2020), 115865, https://doi.org/10.1016/j.applthermaleng.2020.115865.

[27] Y. Sun, G. Di, J. Wang, X. Wang, W. Wu, Performance analysis of R1234yf/ionic liquid working fluids for single-effect and compression-assisted absorption refrigeration systems, Int. J. Refrig. 109 (2020) 25–36, https://doi.org/10.1016/j.ijrefrig.2019.10.007.

[28] M. Wang, T.M. Becker, C.A. Infante Ferreira, Assessment of vapor–liquid equilibrium models for ionic liquid based working pairs in absorption cycles, Int. J. Refrig. 87 (2018) 10–25, https://doi.org/10.1016/j.ijrefrig.2017.09.021.

[29] S. Kim, P.A. Kohl, Theoretical and experimental investigation of an absorption refrigeration system using R134/[bmim][PF6] working fluid, Ind. Eng. Chem. Res. 52 (2013) 13459–13465, https://doi.org/10.1021/ie400985c.

[30] X. Liu, L. Bai, S. Liu, M. He, Vapor−liquid equilibrium of R1234yf/[HMIM][Tf2N] and R1234ze(E)/[HMIM][Tf2N] working pairs for the absorption refrigeration cycle, J. Chem. Eng. Data 61 (2016) 3952–3957, https://doi.org/10.1021/acs.jced.6b00731.

[31] W. Chen, Y. Bai, Thermal performance of an absorption-refrigeration system with [emim]Cu2Cl5/NH3 as working fluid, Energy 112 (2016) 332–341, https://doi.org/10.1016/j.energy.2016.06.093.

[32] W. Chen, S. Liang, Thermodynamic analysis of absorption heat transformers using [mmim]DMP/H2O and [mmim]DMP/CH3OH as working fluids, Appl. Therm. Eng. 99 (2016) 846–856, https://doi.org/10.1016/j.applthermaleng.2016.01.135.

[33] S. Popp, A. Bösmann, R. Wölfel, P. Wasserscheid, Screening of ionic liquid/H2O working pairs for application in low temperature driven sorption heat pump systems, ACS Sustain. Chem. Eng. 3 (2015) 750–757, https://doi.org/10.1021/acssuschemeng.5b00062.

[34] W. Chen, S. Liang, Y. Guo, D. Tang, Thermodynamic analysis of an absorption system using [bmim]Zn 2Cl5/NH3 as the working pair, Energy Convers. Manag. 85 (2014) 13–19, https://doi.org/10.1016/j.enconman.2014.05.024.

[35] E. Vercher, A.V. Orchillés, P.J. Miguel, A. Martínez-Andreu, Volumetric and ultrasonic studies of 1-ethyl-3-methylimidazolium trifluoromethanesulfonate ionic liquid with methanol, ethanol, 1-propanol, and water at several temperatures, J. Chem. Eng. Data. 52 (2007) 1468–1482, https://doi.org/10.1021/je7001804.

[36] W. Chen, C. Xu, H. Wu, Y. Bai, Z. Li, B. Zhang, Energy and exergy analyses of a novel hybrid system consisting of a phosphoric acid fuel cell and a triple-effect compression–absorption refrigerator with [mmim]DMP/CH3OH as working fluid, Energy 195 (2020), 116951, https://doi.org/10.1016/j.energy.2020.116951.

[37] Y. Wang, N. Li, C. Luo, Thermodynamic performance of absorption-compression hybrid refrigeration cycles based on lithium nitrate+1-butyl-3-methylimidazolium nitrate/water working fluid, Int. J. Energy Res. 44 (2020) 10394–10413, https://doi.org/10.1002/er.5661.

[38] C. Song, X. Liu, Z. Ye, M. He, A new power/cooling cogeneration system using R1234ze(E)/ionic liquid working fluid, Int. J. Energy Res. (2020) 1–14, https://doi.org/10.1002/er.5252.

[39] W. Chen, Q. Sun, Y. Bai, B. Zhang, Numerical investigation of the thermal performance of compressor-assisted double-effect absorption refrigeration using [mmim]DMP/CH3OH as working fluid, Energy Convers. Manag. 166 (2018) 433–444, https://doi.org/10.1016/j.enconman.2018.04.060.

[40] S. Kim, P.A. Kohl, Analysis of [hmim][PF6] and [hmim][Tf2N] ionic liquids as absorbents for an absorption refrigeration system, Int. J. Refrig 48 (2014) 105–113, https://doi.org/10.1016/j.ijrefrig.2014.09.003.

[41] W. Wu, T. You, M. Leung, Screening of novel water/ionic liquid working fluids for absorption thermal energy storage in cooling systems, Int. J. Energy Res. 44 (2020) 9367–9381, https://doi.org/10.1002/er.4939.

[42] W. Wu, M. Leung, Z. Ding, H. Huang, Y. Bai, L. Deng, Comparative analysis of conventional and low-GWP refrigerants with ionic liquid used for compression-assisted absorption cooling cycles, Appl. Therm. Eng. 172 (2020) 115145, https://doi.org/10.1016/j.applthermaleng.2020.115145.

[43] B.H. Gebreslassie, M. Medrano, D. Boer, Exergy analysis of multi-effect water-LiBr absorption systems: from half to triple effect, Renew. Energy. 35 (2010) 1773–1782, https://doi.org/10.1016/j.renene.2010.01.009.

[44] T. Avanessian, M. Ameri, Energy, exergy, and economic analysis of single and double effect LiBr-H2O absorption chillers, Energy Build 73 (2014) 26–36, https://doi.org/10.1016/j.enbuild.2014.01.013.

[45] L. Garousi Farshi, S. Asadi, Ammonia lithium nitrate and ammonia sodium thiocyanate double effect absorption refrigeration systems: thermodynamic analysis, Appl. Therm. Eng. 138 (2018) 374–385, https://doi.org/10.1016/j.applthermaleng.2018.04.079.

[46] N.A. Mali, S.S. Bhagwat, Mapping of optimum operating condition for LiBr???water refrigeration cycles, Sadhana - Acad. Proc. Eng. Sci. 42 (2017) 257–269, https://doi.org/10.1007/s12046-017-0597-9.

[47] M. Farshad, Moradi Kashkooli Mohsen, Rezaeian Mostafa, Sefidgar Madjid, Soltani Mostafa, Performance evaluation of series and parallel two-stage absorption chillers driven by solar energy: energetic viewpoint, gas process, J 7 (2020) 77–90.

[48] L. Garousi Farshi, S. Asadi, Ammonia lithium nitrate and ammonia sodium thiocyanate double effect absorption refrigeration systems: thermodynamic analysis, Appl. Therm. Eng. 138 (2018) 374–385, https://doi.org/10.1016/j.applthermaleng.2018.04.079.

[49] L. Dong, D. Zheng, N. Nie, Y. Li, Performance prediction of absorption refrigeration cycle based on the measurements of vapor pressure and heat capacity of H2O +[DMIM]DMP system, Appl. Energy. 98 (2012) 326–332, https://doi.org/10.1016/j.apenergy.2012.03.044.

[50] G. Takalkar, A.K. Sleiti, Comprehensive performance analysis and optimization of 1,3-dimethylimidazolylium dimethylphosphate-water binary mixture for a single effect absorption refrigeration system, Front. Energy. (2021) https://doi.org/10.1007/s11708-021-0720-9.

[51] S.A. Mousavi, M. Mehrpooya, A comprehensive exergy-based evaluation on cascade absorption-compression refrigeration system for low temperature applications - exergy, exergoeconomic, and exergoenvironmental assessments, J. Clean. Prod. 246 (2020), 119005, https://doi.org/10.1016/j.jclepro.2019.119005.

[52] S. Mohtaram, M. Omidi, J. Lin, H. Sun, W. Chen, Exergy analysis of a multi mixture working fluid absorption refrigeration cycle, Case Stud. Therm. Eng. 15 (2019), https://doi.org/10.1016/j.csite.2019.100540.

[53] R. Shirmohammadi, B. Ghorbani, M. Hamedi, M.H. Hamedi, L.M. Romeo, Optimization of mixed refrigerant systems in low temperature applications by means of group method of data handling (GMDH), J. Nat. Gas Sci. Eng. 26 (2015) 303–312, https://doi.org/10.1016/j.jngse.2015.06.028.

[54] G.D. Takalkar, R.R. Bhosale, N.A. Mali, S.S. Bhagwat, Thermodynamic analysis of EMISE–Water as a working pair for absorption refrigeration system, Appl. Therm. Eng. 148 (2019) 787–795, https://doi.org/10.1016/j.applthermaleng.2018.11.092.

[55] W. Wagner, A. Pruß, The IAPWS formulation 1995 for the thermodynamic properties of ordinary water substance for general and scientific use, J. Phys. Chem. Ref. Data. 31 (2002) 387–535, https://doi.org/10.1063/1.1461829.

[56] Z. He, Z. Zhao, X. Zhang, H. Feng, Thermodynamic properties of new heat pump working pairs: 1,3-Dimethylimidazolium dimethylphosphate and water, ethanol and methanol, Fluid Phase Equilib 298 (2010) 83–91, https://doi.org/10.1016/j.fluid.2010.07.005.

[57] J. Pátek, J. Klomfar, A computationally effective formulation of the thermodynamic properties of LiBr-H2O solutions from 273 to 500 K over full composition range, Int. J. Refrig. 29 (2006) 566–578, https://doi.org/10.1016/j.ijrefrig.2005.10.007.

[58] K. Mahalle, P. Parab, S. Bhagwat, Optimization of cooling load in the combined vapour absorption–vapour compression refrigeration cycle using exergy analysis, Indian Chem. Eng. 61 (2019) 52–66, https://doi.org/10.1080/00194506.2017.1418439.

[59] B.S. Bagheri, R. Shirmohammadi, S.M.S. Mahmoudi, M.A. Rosen, Optimization and comprehensive exergy-based analyses of a parallel flow double-effect water-lithium bromide absorption refrigeration system, Appl. Therm. Eng. 152 (2019) 643–653, https://doi.org/10.1016/j.applthermaleng.2019.02.105.